Catalysis Science & Technology

Accepted Manuscript

ROYAL SOCIETY OF CHEMISTRY

www.rsc.org/catalysis

Hierarchically shape-controlled mixed-valence calcium manganites for catalytic ozonation of aqueous phenolic compounds

Yuxian Wang[1,2], Yongbing Xie[1], Hongqi Sun[2], Jiadong Xiao[1], Hongbin Cao[1] and Shaobin Wang[2]**

[1]Beijing Engineering Research Center of Process Pollution Control, Key Laboratory of Green Process and Engineering, Institute of Process Engineering, Chinese Academy of Sciences, Beijing 100190, China. Email: ybxie@ipe.ac.cn (Y. X)

[2]Department of Chemical Engineering, Curtin University, GPO Box, U1987, Perth, WA 6845, Australia. Email: shaobin.wang@curtin.edu.au (S.W)

ABSTRACT

Catalytic ozonation has attracted intensive attention due to its efficient degradation of various organic pollutants in water. The key to a practical application is the discovery of highly effective catalysts. This study, for the first time, reports excellent performances of porous mixed-valence calcium manganite ($CaMn_3O_6$ and $CaMn_4O_8$) microspheres made of 1D nanorods in catalytic ozonation of 4-nitrophenol. The $CaMn_3O_6$ and $CaMn_4O_8$ showed much higher activities and stabilities than manganese oxides. From a variety of advanced characterizations, the mechanism of surface catalysis was discussed in-detail. Several quenching reagents and electron paramagnetic resonance (EPR) were applied to probe the dominant reactive species in the catalytic ozonation over the calcium manganites. It was found that superoxide radicals and singlet oxygen other than hydroxyl radicals contributed to the degradation and mineralization of 4-nitrophenol. Moreover, the effects of electron-withdrawing group (EWG) and electron-donating group (EDG) in phenolic compounds on ozonation/catalytic ozonation over the calcium manganites were investigated using phenol, p-cresol and p-chlorophenol as target pollutants.

Keywords: Catalytic ozonation, calcium manganese oxides, 4-nitrophenol, organic pollutants, reactive radicals

1 Introduction

In the past few decades, manganese-based materials have attracted worldwide attention and presented humongous potentials in energy storage, catalysis and electrode materials attributing to the unique physicochemical properties, low cost and less toxicity.[1-4] In terms of catalysis, their structural flexibility with potential incorporation of other metals has offered promising opportunities for regulating their physicochemical properties and catalytic activity.[5] Recently, mixed valence manganites have appeared to be more interesting than conventional manganese oxides because of their superior chemical and physical properties.[2, 6, 7] Lee et al. synthesized a novel heterostructured spinel $LiMn_2O_4$ and explored its application as cathode materials for Li-ion battery.[7] It was found that this novel spinel-layered structure hindered the manganese dissolution and offered an efficient flow path for ions and electrons. However, most of the current research efforts focused on the electrocatalysis relating to energy storage, while very limited investigations in chemical catalysis for environmental remediation have been reported.

Nitroaromatic compounds have been widely and consistently discharged into the environment from industrial production processes of various chemicals such as insecticides, pesticides, synthetic dyes, and pharmaceuticals.[8, 9] 4-Nitrophenol as one of the nitroaromatic compounds was recognized as a priority pollutant by the U.S. EPA, and has shown high toxicity, mutagenic and carcinogenic effects on both human beings and natural lives.[9] Moreover, the strong electron-withdrawing nitro group in the aromatic ring makes 4-nitrophenol more recalcitrant to be degraded by traditionally chemical or biological treatments.[10]

In recent years, advanced oxidation processes (AOPs) employing reactive species for degradation of aqueous organic pollutants have presented a high efficiency and exceptional mineralization capability for environmental remediation.[11] Among AOPs, Fenton/Fenton-like reactions via hydroxyl radicals (E_0 = 2.7 V) have been proven as one of cost-effective technologies,[12] while metal leaching, sludge production and low pH range (< 4) place the barricade to their further applications.[13] Compared to Fenton reaction, reactive species such

as $^{\cdot}OH$, $^{1}O_2$ and $^{\cdot}O_2^{-}$ can been produced from activation of ozone for the degradation of persistent organic pollutants.[14, 15] Traditional ozonation process is effective for removal of organic compounds containing multiple bonds such as C=C and C=N. However, the slow reaction rate and partial mineralization of aromatic compounds hinder its wide implementation.[14] By contrast, catalytic ozonation using an effective catalyst successfully circumvents these drawbacks. Not only has controlled decomposition of ozone been achieved, but also the generated active radicals would be highly responsible for efficient mineralization of persistent organic contaminants.[15-17] In addition, solution pH for the oxidation reactions can be adjusted in accordance to the properties of catalysts.[17, 18]

Transition metal ions such as Mn(II), Fe(II), Co(II) and Cu(II) have demonstrated high efficiencies in catalytic ozonation for homogeneous degradation of various organic pollutants.[19-21] However, secondary pollution brought by the heavy metal ions poses risks to both human beings and the environment. More recently, heterogeneous catalysts such as modified activated carbon,[17, 22] metal oxides[23, 24] and supported metal oxides[18, 25] have been attempted for catalytic ozonation showing high activities. Manganese oxides, with prolific existence on the earth and low toxicity to the environment, have been extensively employed as promising catalysts for catalytic ozonation due to the unique chemical state variation cycle inducing from the single electron transfer.[26, 27] Recently, multivalent MnO_x has attracted intensive research interests since the involved two redox couples (Mn^{4+}/Mn^{3+} and Mn^{3+}/Mn^{2+}) would promote the electron transfer and thus resulting in a higher catalytic activity.[28-30] Nevertheless, mesoporous supports such as α-Al_2O_3 were employed for these multivalent MnO_x catalysts to enhance the catalytic stability. For catalytic ozonation of aqueous organic pollutants, it has been confirmed that addition of calcium ions could significantly improve the total organic carbon (TOC) removal rate by binding with reaction intermediates to form insoluble precipitates.[31] However, very few researches reported calcium involved heterogeneous catalysts in catalytic ozonation processes.

In this study, two mixed valence calcium manganites of $CaMn_3O_6$ and $CaMn_4O_8$ in 3D hierarchical structure made of 1D sub-blocks were synthesized via a facile calcination

method using cation carbonate precursors. For the very first time, calcium involved mixed valence manganites for catalytic ozonation was reported. The catalytic performances of the materials were investigated by catalytic ozonation of 4-nitrophenol, which is one of the main discharged pollutants from pharmaceutical, pesticide and dye production industries.[32] With addition of quenching agents and electron paramagnetic resonance, the dominant active species for 4-nitrophenol degradation were identified. Moreover, the pollutants containing electron-withdrawing group (EWG) and electron-donating group (EDG) in the aromatic structure were further evaluated in the catalytic ozonation using phenol, 4-chlorophenol and p-cresol.

2 Experimental methods

2.1 Materials and chemicals

Calcium carbonate (99.5%), ammonium carbonate (99%) and manganese carbonate (99.8%), 5,5-Dimethyl-1-pyrroline (DMPO) and 2,2,6,6-tetramethyl-4-piperidone (TEMP) were obtained from Sigma-Aldrich. Nitric acid (70%) was purchased from Chem-Supply. p-Benzoquinone (99.0%) was procured from Alfa Asar, *tert*-butanol (*t*-BA, 99.0%) and sodium azide (NaN_3, 99.0%) were purchased from Sinopharm Chemical Reagent Co. Ltd. 4-Nitrophenol (99.5%) was purchased from Aladdin Reagent. A commercial MnO_2 was obtained from Beijing Chemical Plant, China.

2.2 Synthesis of mixed-valence calcium manganites

Calcium manganese oxides were synthesized via a modified co-precipitation method. For synthesis of $CaMn_3O_6$, 10 mmol $CaCO_3$ and 30 mmol $MnCO_3$ were dissolved in 80 mL diluted nitric acid (1 M). With vigorous stirring, 200 mL of 2 M ammonium carbonate solution was added into the mixed cation solution to make the solution pH > 8. A brownish precipitate was harvested by vacuum filtration followed by washing with ultrapure water for three times. Then the precipitate was dried at 100 ^oC in an oven overnight. After that the dried precipitate was transferred into a crucible and heated in a muffle furnace in air at 800 ^oC for 18 h and the obtained black powder was denoted as $CaMn_3O_6$. $CaMn_4O_8$ was synthesized via the similar method except for the $MnCO_3$ dosage at 40 mmol. Meanwhile,

manganese oxide was prepared from the similar synthesis procedures without the addition of calcium source.

2.3 Characterization of materials

Field emission scanning electron microscopy (FESEM, ZEISS NEON 40EsB) with energy dispersive spectroscopy (EDS) was employed to observe the structure and morphology of the as-synthesized calcium manganite samples. X-ray diffraction (XRD) patterns of the samples were acquired by X'Pert-PROMPD (PAN analytical B.V.), operating at an accelerated voltage of 40 kV and an emission current of 40 mA with Cu Kα radiation (λ = 1.5418 Å). N_2 adsorption/desorption isotherm at -196 ^{o}C (Autosorb-iQ, Quantachrome) was utilized to obtain the Brunauer–Emmett–Teller (BET) specific surface areas and the pore size distributions of the samples from the BET and density functional theory (DFT) methods, respectively.[33] The samples were degassed at 200 ^{o}C for 8 h prior to testing. Surface chemical composition of the samples was determined by X-ray photoelectron microscopy (XPS, Thermo Fisher Scientific ESCALAB 250Xi) under ultra-high vacuum (UHV) condition with Al-Kα X-ray. Spectra were fitted with CasaXPS software. Transmission electron microscopy (TEM) images were obtained from a JEOL 2100F (UHR) TEM instrument.

2.4 Catalytic ozonation processes

Catalytic ozonation processes were carried out in a semi-batch reactor containing 0.5 L of the target pollutant. Submerged in a water bath, the reactor temperature was controlled at 25 ^{o}C constantly with a stirring speed of 300 rpm. Ozone was generated from high purity oxygen (99.9%) by an Anseros Ozomat GM ozone generator. The inlet flow rate of ozone was 100 mL/min at the concentration of 50 mg/L which was monitored by the Anseros Ozomat GM ozone detector. In a typical test, 0.05 g catalyst was added into the target pollutant solution which was kept stirring for 30 min to achieve adsorption-desorption equilibrium. Then the valve connecting to the ozone generator was opened to feed ozone into the bottom of the reactor through a porous glass-made diffuser. At certain time intervals, water samples were withdrawn from the reactor with a syringe and filtered into a HPLC vial via a 0.45 μm PTFE filter. Concentrations of the pollutants were investigated by high performance liquid

chromatography (HPLC, Agilent Series 1200) with a UV detector set at the wavelength of 220 nm and a C-18 column. The mobile phase was made of 70% of diluted phosphate acid (1 wt%) and 30% of methanol solution at a flow rate of 0.25 mL/min. Total organic carbon (TOC) of the withdrawn water samples was determined by a Shimadzu TOC-vcph analyzer. For stability tests, the used catalyst sample was collected by vacuum filtration after each run and cleaned with ultrapure water for 3 times. Catalytic ozonation experiments were repeated in order to obtain error bars on the plots. Electron paramagnetic resonance (EPR) experiments for radical analysis were performed on a Bruker EMX-E spectrometer (Germany) with DMPO and TEMP as spin-trapping agents.

3 Results and discussion

3.1 Characterization of the materials

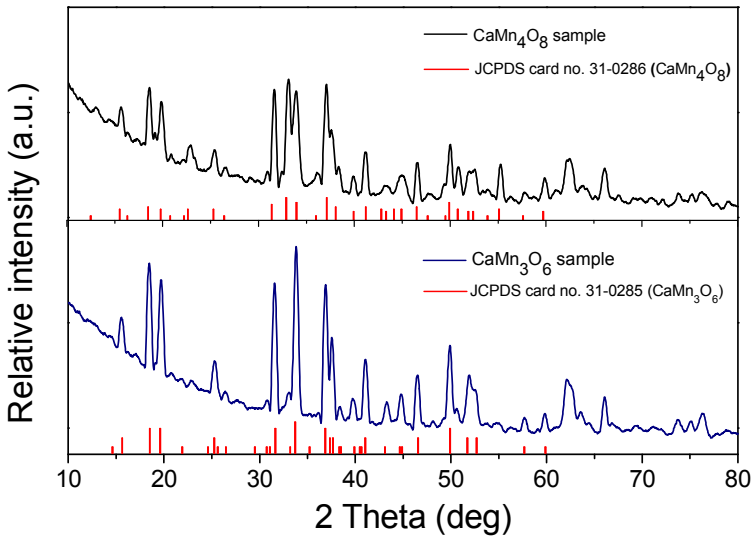

Figure 1. XRD patterns of Ca-Mn-O samples.

X-ray diffraction patterns of two Ca-Mn-O samples (Fig.1) shows good agreements with the profiles of monoclinic $CaMn_3O_6$ (JCPDS card no. 31-0285) and orthorhombic $CaMn_4O_8$ (JCPDS card no. 31-0286), respectively. Moreover, no diffraction peaks from other phases were detected, confirming a high purity of the two samples. It was reported that $CaMn_3O_6$ is constructed by the rutile-type chain of edge-sharing MnO_6 octahedra, which are connected by double chains, and that the six-sided tunnels produced by interlinking of the common corners

of the chains provide a unique space for accommodation of Ca^{2+} ions.[6, 34] While $CaMn_4O_8$ has a slightly different crystal structure. Although $CaMn_4O_8$ also possesses a tunnel structure, it is built up by a framework of both single and triple chains of edge-sharing MnO_6 octahedra, which are interconnected by the common corners.[34] Moreover, the infinite sheets of $[Mn_4O_8]^{2-}$ supplies three types of tunnel for Ca^{2+} cations to reside in.[35] These differences in the crystal structures would give rise to variations of physical and chemical properties of these Ca-Mn-O compounds. Meanwhile, manganese oxide was prepared under the same synthesis procedures as Ca-Mn-O catalysts without addition of calcium source. XRD analysis (ESI Fig. S1†) suggested that Mn_2O_3 with the crystal structure of *la-3* (JCPDS card no. 65-7456) was formed, obtaining a single valence state of Mn (+3). Calcium ions within these Ca-Mn-O catalysts are responsible for stabilizing high valence state manganese. Without the presence of calcium, only Mn^{3+} would remain at high synthesis temperature (above 800 ^oC). In addition, the morphology of the as-synthesized manganese oxide observed from SEM image (ESI Fig.S2†) was quite different from Ca-Mn-O, revealing the key role of Ca for functional assembly of $[Mn_4O_8]$ framework.[36, 37]

The morphologies of the Ca-Mn-O samples were examined by FESEM and TEM (Fig.2). $CaMn_3O_6$ presented as a hierarchical 3D microsphere (1.5-2 μm in diameter) constructed by 1D nanorods with the average length of 0.5 μm (Fig.2 (A) and (B)). $CaMn_4O_8$ displayed the similar hierarchical structure to $CaMn_3O_6$ (Fig.2 (C) and (D)), but with a smaller diameter and less sphericity, constructed by less tightly built 1D nanorods in irregular length ranging between 200-500 nm. The difference in the morphology of these Ca-Mn-O samples might be ascribed to the disparity in synthesis conditions. For $CaMn_4O_8$, the more amount of $MnCO_3$ precursor favored the synthesis of 1D nanorod structure. Also the increased amount of CO_3^{2-} would be decomposed at an elevated temperature to facilitate the formation of loose microspheres with rough surface.[5]

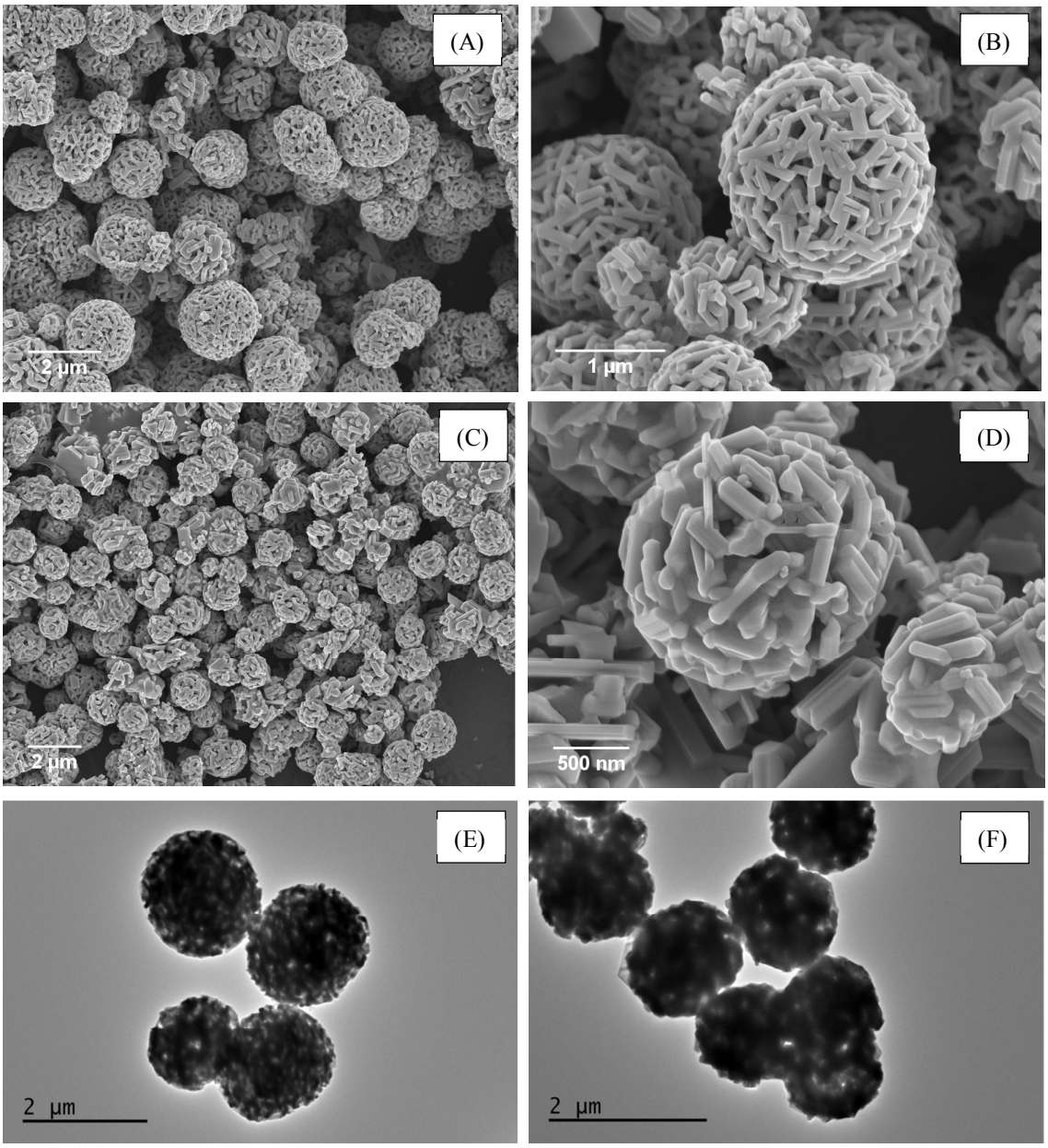

Figure 2. SEM images of $CaMn_3O_6$ (A and B) and $CaMn_4O_8$ (C and D), and TEM images of $CaMn_3O_6$ (E) and $CaMn_4O_8$ (F).

TEM images of these samples (Fig.2 (E) and (F)) show that the morphology and the primary particle size were in an agreement with those in SEM images. Some bright dots within the microspheres in TEM images suggest the existence of porous structure within the samples.

The phase transition from low-density carbonate precursors to high-density oxides with the evaporation of carbon dioxide and the Ostwald ripening of agglomerated particles with the production of perovskite structures might be the two reasons for the formation of this porous structure inside the hierarchical microspheres.[38] EDS (ESI Fig. S3† (A and B)) describes the atomic compositions of these two samples, in terms of Ca, Mn and O elements. The atomic ratios of Ca, Mn and O for $CaMn_3O_6$ and $CaMn_4O_8$ were 1:3.1:6.2 and 1:4.0:8.1, respectively, in a good agreement with their corresponding chemical structures. While the unlabeled peaks belong to Al and Si generated from SEM stubs.

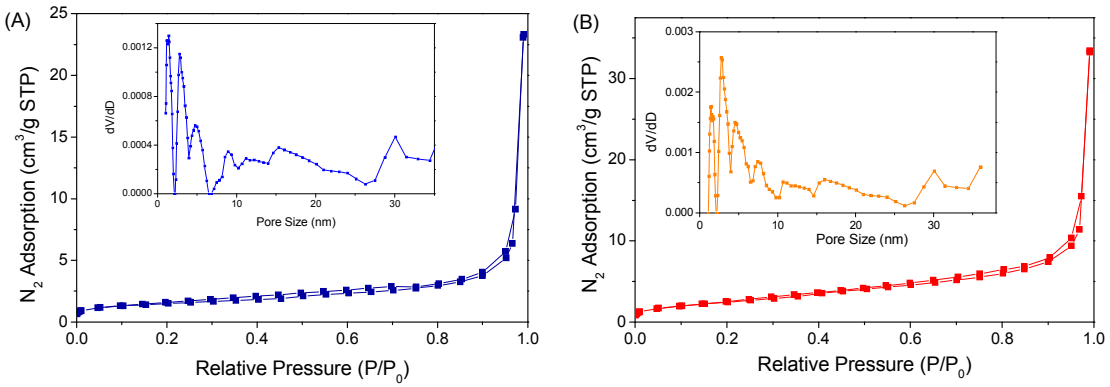

Figure 3. Nitrogen sorption isotherms and pore size distributions of $CaMn_3O_6$ (A) and $CaMn_4O_8$ (B).

Fig. 3 presents N_2 sorption isotherms of the Ca-Mn-O samples. Both $CaMn_3O_6$ and $CaMn_4O_8$ samples demonstrated a type IV isotherm with a type H3 hysteresis loop indicating a mesoporous structure.[39] $CaMn_4O_8$ presented higher a BET specific surface area (8.8 vs. 5.3 m^2/g) and total pore volume (0.052 vs. 0.036 cm^3/g) than $CaMn_3O_6$ (Table 1), which was also validated by higher N_2 adsorption and the broader hysteresis loop of $CaMn_4O_8$ ranging from 0.25 to 0.99 of the relative pressure P/P_0. For $CaMn_4O_8$, the more porous structure could be ascribed to the evaporation of higher amount of carbon dioxide from the carbonate precursors. In terms of pore size, the as-synthesized samples displayed a multi-modal pore size distribution, in which both micropores and mesopores were identified and the average pore diameters for $CaMn_3O_6$ and $CaMn_4O_8$ were 23.3 and 27.4 nm, respectively.

Table 1. Textural properties of Ca-Mn-O catalysts and reaction kinetics in 4-nitrophenol degradation.

Catalyst	Surface area (S_{BET} m^2/g)	Pore volume (cm^3/g)	Average pore diameter (nm)	First-order rate constant (min^{-1})	R^2
$CaMn_3O_6$	5.3	0.036	23.3	0.113	0.992
$CaMn_4O_8$	8.8	0.052	27.4	0.125	0.995

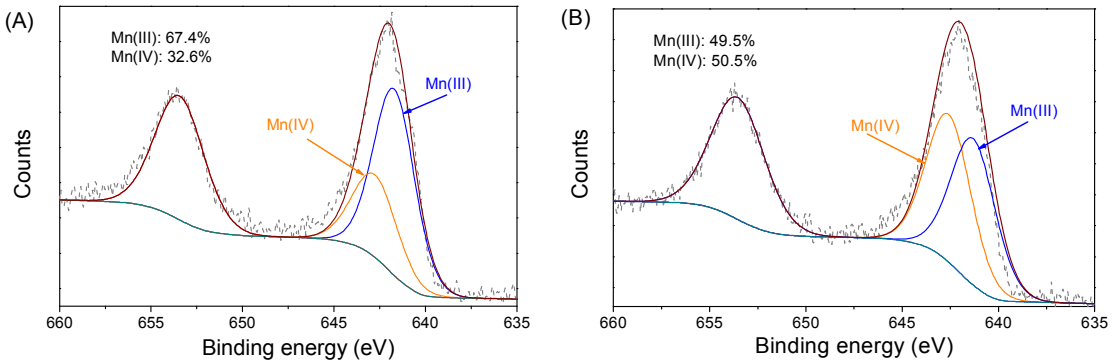

Figure 4. XPS spectra of Mn 2p region for $CaMn_3O_6$ (A) and $CaMn_4O_8$ (B).

For mixed-valence manganites like $CaMn_3O_6$ and $CaMn_4O_8$, the valence transition of Mn would be the active sites for catalytic reactions.[3, 40] In order to determine the chemical state of Mn, XPS spectra of Mn 2p region for $CaMn_3O_6$ and $CaMn_4O_8$ were examined (Fig. 4). For both the samples, two characteristic peaks centering at around 642 and 653 eV were observed, which could be ascribed to Mn $2p_{3/2}$ and Mn $2p_{1/2}$ spin-orbit doublet, respectively. For $CaMn_3O_6$, the peak of Mn $2p_{3/2}$ was centered at 641.8 eV, while it was shifted to 642.2 eV for $CaMn_4O_8$, indicating the composition change of the Mn valence, driven by the decrease in 3d count.[41] To further investigate the changes, the Mn $2p_{3/2}$ peaks for $CaMn_3O_6$ and $CaMn_4O_8$ were split and curve-fitted. In accordance with previous studies,[42, 43] the peaks at 641.4 and 641.7 eV could be assigned to Mn(III) for $CaMn_3O_6$ and $CaMn_4O_8$, respectively, and the peaks at 642.4 eV for $CaMn_3O_6$ and 642.8 eV for $CaMn_4O_8$ were ascribed to Mn(IV). The

Mn states of $CaMn_3O_6$ were made of 67.4% of Mn(III) and 32.6% of Mn(IV). The ratio of Mn (III) to Mn(IV) (2:1) was quite close to the nominal distribution of Mn valence within $CaMn_3O_6$, and thereby, $CaMn_3O_6$ could be regarded as $CaMn(III)_2Mn(IV)O_6$ with the average Mn valence of 3.27. While for $CaMn_4O_8$, the Mn(IV) composition was elevated to 50.5%, enabling the average Mn valence to be 3.52. The distribution of Mn valence within $CaMn_4O_8$ was calculated to be $CaMn(III)_2Mn(IV)_2O_8$. Previous works revealed that the average valence of Mn on the surface of a MnO_x based catalyst situating between 3+ and 4+ usually possessed a higher catalytic activity. [5]

3.2 Catalytic ozonation of 4-nitrophenol

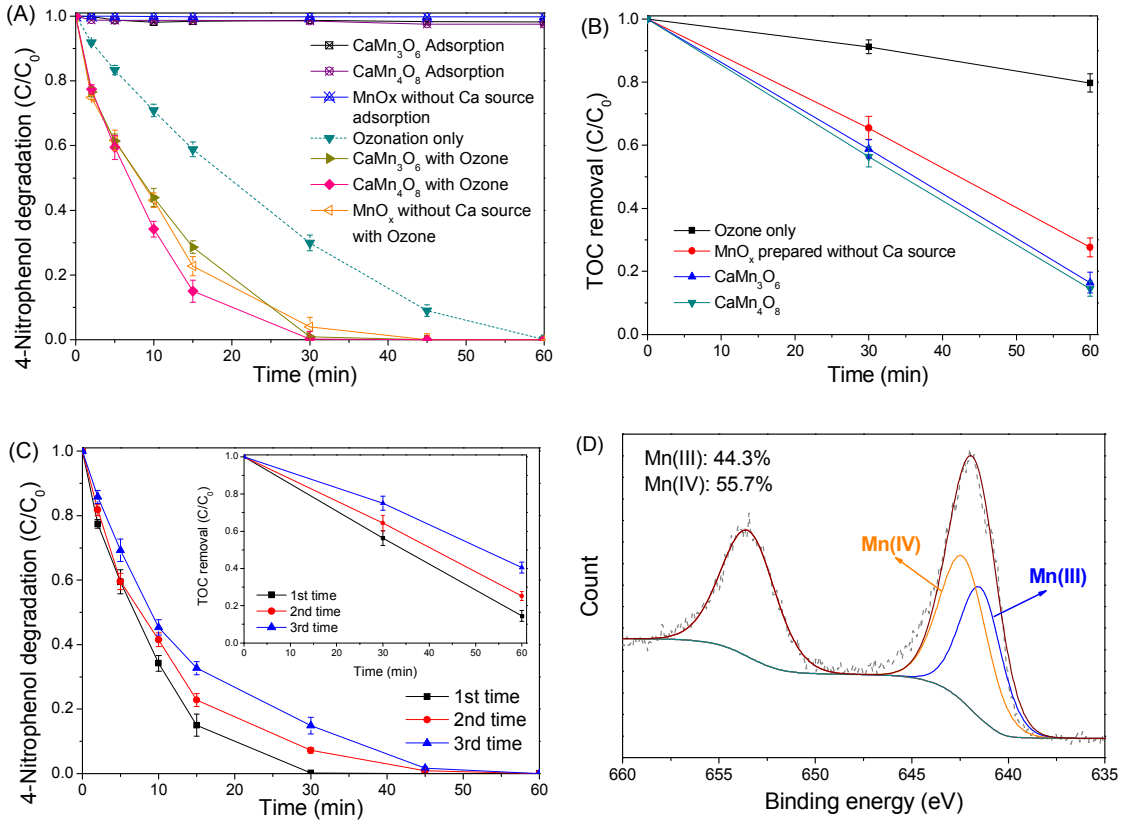

Figure 5. (A) Catalytic ozonation of 4-nitrophenol with various catalysts and the corresponding TOC removal (B). (C) Successive reusability tests for 4-nitrophenol degradation and the corresponding TOC removal (inset). (D) XPS spectra of Mn 2p region for used $CaMn_4O_8$ catalyst. Reaction conditions: $[4\text{-nitrophenol}]_0$ = 50 mg/L, Catalyst loading = 0.1 g/L, Ozone flow rate: 100 mL/min, Ozone loading: 50 mg/L, Temperature: 25

^{o}C, Solution pH=5.7.

Fig. 5 displays adsorption and catalytic ozonation of 4-nitrophenol on various samples. As seen, for both Ca-Mn-O samples, adsorption led to marginal 4-nitrophenol removal at less than 3% in 1 h. For ozonation, 4-nitrophenol was nearly decomposed in 1 h suggesting a high oxidation efficiency of ozone. However, more than 80% of total organic carbon still remained in the solution, revealing low mineralization (Fig.5(B)). With the contribution of the catalyst, 4-nitrophenol degradation profile (Fig. 5(A)) was more concave compared with that in ozonation, implying a faster reaction rate. The TOC removal increased from 20% to 50%, suggesting more organic pollutants were oxidized into carbon dioxide and water. Complete 4-nitrophenol removal efficiencies were achieved within 45 and 30 min on $CaMn_3O_6$ and $CaMn_4O_8$, respectively. While both of the catalysts demonstrated quite similar TOC removal efficiencies at around 82% in 1 h. In order to provide the benchmark for catalytic activities of the as-prepared Ca-Mn-O materials, control experiments were carried out employing manganese oxide prepared without Ca source and commercial MnO_2 (ESI Fig. S5†). As seen, manganese oxide prepared without Ca source demonstrated a similar catalytic activity for 4-nitrophenol degradation as Ca-Mn-O, while an inferior TOC removal rate. Meanwhile, the commercial MnO_2 demonstrated a much lower rate for both 4-nitrophenol degradation and TOC removal.

For heterogeneous catalytic ozonation on manganese-based catalysts, it was reported that surface manganese would dissolve into the reaction solution to initiate the homogeneous catalytic ozonation and improve the reaction rate.[25, 44] Inductively coupled plasma (ICP, Optima 6300DV, Perkin Elmer) results showed that, for manganese oxide synthesized without a calcium source, more than 10 ppm of Mn ions remained within the solution after 60 min of reaction time, and the leached Mn ions would induce a strong homogeneous catalytic reaction which contributed to 4-nitrophenol decomposition. However, for Ca-Mn-O catalysts, Mn ion concentration after each reaction was examined to be well below 2 ppm, not only revealing an insignificant leaching problem, but also suggesting that, with the presence of calcium, Mn ions are more stable within the Ca-Mn-O structure. In addition, the contribution

of the leached Mn ions as homogeneous catalysts to the reaction was evaluated (ESI Fig. S6†). A negligible catalytic activity was observed in 4-nitrophenol degradation and TOC removal when 2 ppm Mn^{2+} was applied. Nevertheless, 10 ppm of Mn^{2+} brought about a significant homogenous catalytic effect.

ICP analyses also indicated around 2 ppm of Ca^{2+} was dissolved in the solution after the reaction. And the influence of Ca ions on catalytic ozonation performance has been investigated by utilizing Ca^{2+} (from $Ca(NO_3)_2$) as the homogeneous catalyst. As seen in Fig. S7† (ESI), addition of 2 ppm of Ca^{2+} could slightly increase the catalytic ozonation efficiency for 4-nitrophenol degradation, however, TOC removal rate was boosted. A previous study revealed that the presence of Ca^{2+} would not affect the ozonation pathway, while it would bind with reaction intermediates to form insoluble solids which were responsible for TOC removal.[31]

Solution pH plays a crucial role in the catalytic ozonation process by influencing the decomposition rate of ozone.[45-47] It is well acknowledged that higher pH favors the decomposition of ozone molecules. In addition, mass transfer rate between ozone and water is affected by the solution pH. To probe the influence of mass transfer in our catalytic ozonation system, ozone concentrations in off-gas and liquid phase were measured by the Anseros Ozomat GM ozone detector and indigo method,[48] respectively.

Fig. S8† (ESI) describes the variations of ozone concentrations in liquid phase and off-gas from ultrapure water at pH 5.7. Without a catalyst and target pollutant, both ozone mass transfer equilibria in liquid phase and off-gas were achieved after 5 min of bubbling. And it was found aqueous ozone concentration was around 5 mg/L. In 50 ppm of 4-nitrophenol solution without the catalysts (ESI Fig. S9†), ozone mass transfer equilibrium in the off-gas was reached within 7 min and the ozone absorption in the liquid phase remained at rather low values (<0.5 mg/L) throughout the reaction time. Fig. S10† (ESI) displays the variations of ozone concentrations in off-gas and liquid phase for catalytic ozonation process. Similar to the profiles in ozonation process, the low ozone concentration in the liquid phase could be

ascribed to the fast reaction between the absorbed ozone molecules and the aromatic pollutants. And this trend was well in accordance to the catalytic ozonation profile of 4-nitrophenol, in which complete degradation of 4-nitrophenol was achieved within 30 min.

After 30 min of reaction, ozone concentration in the liquid phase began to increase and finally reached equilibrium at 50 min, suggesting that the target pollutant as well as most of the aromatic intermediates were degraded in 30 min. After that the active species generated by decomposition of the ozone would be responsible for further degradation and mineralization of the reaction intermediates, especially for those containing multiple bonds, which were reflected in the further reduction of TOC after 30 min (Fig. 5(B)).

Beltran et al. discovered that the regime of ozone absorption in water becomes successively faster at the increased solution pH level: very slow at pH < 2, slow at pH = 2-6.5, fast at pH=6.5 and instantaneously at higher pH.[45] Hoigne and Bader obtained the direct ozonation constant of 4-nitrophenol to be 1.4×10^6 $M^{-1}s^{-1}$ at pH = 8, and suggested that instantaneous reaction between 4-nitrophenol and ozone would occur.[46] Compared with the corresponding ozone absorption profile in ultrapure water, the low absorption of ozone in 4-nitrophenol solution indicated that ozone was quickly consumed by the reaction in the acid solution (pH 5.72), little ozone absorption occurred in 4-nitrophenol solution.[45] Therefore, the influence of ozone mass transfer was insignificant in the catalytic ozonation process.

In the previous works, several Ca-Mn-O materials were synthesized, characterized and employed in catalytic applications.[5, 6, 34, 49, 50] Han et al. synthesized a series of $Ca_{1-x}Mn_xO$ samples by thermal decomposition of solid-solution carbonate precursors and investigated their electrocatalytic activities in oxygen reduction reactions (ORR).[6] The study revealed that the as-prepared $CaMnO_3$ and $CaMn_3O_6$ microspheres demonstrated an excellent catalytic activity and yielded low amount of peroxide species in alkaline solutions during the ORR. Barrocas et al. prepared a $CaMn_3O_6$ film and evaluated the photocatalytic decolorization of Rhodamine 6G (Rh6G) under visible light irradiation.[5] The $CaMn_3O_6$ film demonstrated a much higher activity than TiO_2.[5, 51] Compared with the current study, though those Ca-Mn-O

catalysts possessed superior activities, their morphologies were not rigid. In the present study, Ca-Mn-O materials with rigorous 3D hierarchical microspheres made of 1D sub-blocks were successfully prepared. Moreover, for the very first time, the mixed valent Ca-Mn-O samples have been applied for the catalytic ozonation system and showed exceptional activities.

In order to quantify the reaction rate, the degradation profiles were fitted with a pseudo first order kinetic model (Eq. (1)).

$$ln\left(\frac{C}{C_0}\right) = -kt \qquad \text{Equation 1.}$$

Where k is the pseudo first order reaction rate constant. C_0 and C are the concentrations of 4-nitrophenol at initial and time t, respectively. As seen in Fig. S11† (ESI), both 4-nitrophenol degradation in ozonation and catalytic ozonation processes using commercial MnO_2 and Ca-Mn-O catalysts were well fitted by the model with high values of regression coefficient. The reaction rate constants (k) of 4-nitrophenol degradation in ozonation and catalytic ozonation on commercial MnO_2, $CaMn_3O_6$ and $CaMn_4O_8$ were calculated to be 0.039, 0.049, 0.113 and 0.125 min^{-1}, respectively (Table 1). Compared with ozonation process, 4-nitrophenol degradation rate was slightly improved by the commercial MnO_2. When Ca-Mn-O materials were employed, the reaction rate constants increased by more than 2 times, indicating the catalytic activity of these mixed-valence manganese materials is much superior to the single-valence manganese oxide.

It is known that catalytic activity of a material is dependent on the surface area, valence state and crystal structure. The BET specific surface area of the commercial MnO_2 was determined to be 27.9 m^2/g (ESI Fig. S4†), which was greater than that of $CaMn_3O_6$ and $CaMn_4O_8$ samples. The catalytic activity of the commercial MnO_2, however, was much inferior to that of $CaMn_3O_6$ and $CaMn_4O_8$, revealing that the catalytic activity was not dependent on the specific surface area. For MnO_x based materials, the redox reaction occurred in a Mn^{3+}/Mn^{4+} couple involving a single electron transfer is the key factor influencing the catalytic activity.[3, 26] As shown in XPS spectra, the distributions of Mn chemical states for the $CaMn_3O_6$ and $CaMn_4O_8$ are $CaMn(III)_2Mn(IV)O_6$ (with average Mn valence of 3.3) and

$CaMn(III)_2Mn(IV)_2O_8$ (with average Mn valence of 3.5), respectively. The coexistence of Mn^{3+} and Mn^{4+} would promote the generation of more ionic defects (misplaced ions and vacancies) and electronic defects (electrons and holes) and thus speed up the surface redox reactions for catalytic reactions.[2]

Variation of reaction conditions could induce a significant influence on catalytic ozonation efficiency. Fig. S12† (ESI) displays catalytic ozonation efficiencies of $CaMn_4O_8$ at varying initial 4-nitrophenol concentrations. 4-Nitrophenol degradation efficiency decreased with the increase of the initial concentration. At 25, 50 and 100 ppm of initial 4-nitrophenol concentrations, complete removal would be achieved within 15, 30 and 60 min, respectively. And the corresponding TOC removal (inset figure) demonstrated the similar trend. When the initial 4-nitrophenol concentration was elevated to 100 ppm, only 40% TOC removal was achieved, indicating the amount of active species produced in the reaction was not high enough for mineralization of pollutants at a higher 4-nitrophenol concentration.

Fig. S13†(ESI) presents the effect of catalyst loading on catalytic ozonation efficiencies. As seen, a higher amount of catalyst loading could dramatically enhance the catalytic reaction rate. At 0.05 g/L of $CaMn_4O_8$ loading, it would take more than 45 min for 100% degradation of 4-nitrophenol and the corresponding TOC removal was around 70%. However, at 0.1 g/L of catalyst loading, not only the degradation rate became faster, but also the TOC removal was increased to more than 80%. Further increase in the catalyst loading would result in a much faster 4-nitrophenol degradation efficiency. At 0.2 g/L, complete pollutant degradation would be reached in less than 30 min, and nearly 90% of TOC was mineralized in 60 min. Therefore, a higher catalyst loading would generate more active species from ozone and thus lead to a better catalytic ozonation efficiency.

Fig. S14† (ESI) describes the effect of ozone loading on 4-nitrophenol decomposition. A higher ozone loading could result in a higher catalytic ozonation efficiency. At 100 mg/L ozone loading, 100% degradation of 4-nitrophenol could be achieved within 30 min. Nevertheless, at ozone loading of 25 mg/L, complete 4-nitrophenol removal would be

realized at 60 min. When ozone loading was increased from 25 to 50 mg/L, TOC removal was significantly enhanced from 60 to nearly 85%. However, when ozone loading was further increased to 75 mg/L, less than 5% further increase occurred to TOC removal.

Stability and recyclability of the $CaMn_4O_8$ catalyst were evaluated through a three-run successive test wherein the catalyst was collected by vacuum filtration after each run and followed by washing with ultrapure water. Compared with 100% degradation of 4-nitrophenol in 30 min for the fresh catalyst, the time for complete 4-nitrophenol removal in the second and third runs was extended to 45 and 60 min, respectively (Fig. 5(C)). And the corresponding TOC removal was decreased from 82% to 60%. Adsorption of reaction intermediates is reported as one of the deactivation factors of the catalysts. Recent investigations demonstrated that the catalyst activity could be regenerated by ultrasound or heat treatment to remove the physically attached intermediates.[40, 52] However, low BET surface areas of these Ca-Mn-O samples suggested that passivation of the catalysts brought by blockage of the reaction intermediates is insignificant.

Another factor that leads to deactivation of the catalyst might be the composition change, especially the changes of Mn states. XPS spectra of Mn 2p region for the used catalyst were examined (Fig. 5(D)). Compared to the fresh catalyst (Fig. 4(B)), the relative composition of Mn(IV) increased from 50.5% to 55.7%, suggesting around 5% of Mn(III) has been oxidized to Mn(IV) by either ozone or reactive species generated. Previous studies have verified that, for manganese-based catalysts, redox cycles involved in ozone decomposition occurred on the catalyst surface.[28, 53, 54] Lv et al. employed cyclic voltammetry (CV) methods to evaluate the electron transfer behavior of the Mn-based catalysts during the catalytic ozonation process.[54] It was found, when Mn-based materials were utilized as the electrode, a couple of stable and well-defined redox peaks appeared which could be assigned to Mn^{3+}/Mn^{4+} redox cycle. And the single electron transfer involved in this cycle would act as the active sites to trigger the decomposition of ozone molecules to form active oxygen species. [55, 56] Therefore, Mn^{3+}/Mn^{4+} redox couple was proven as the active sites for catalytic reactions. Moreover, the composition change in Mn^{3+}/Mn^{4+} may induce the deactivation or variation of the catalytic

activity. [24]

3.3 Probing active species responsible for 4-nitrophenol degradation

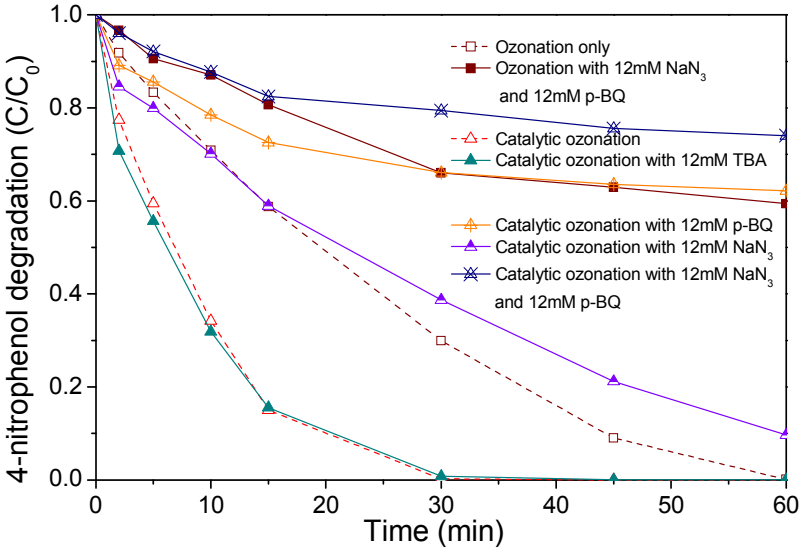

Figure 6. Competitive radical tests for catalytic ozonation of 4-nitrophenol. Reaction conditions: $[4\text{-nitrophenol}]_0$ = 50 mg/L, Catalyst loading = 0.1 g/L, Ozone flow rate: 100 mL/min, Ozone loading: 50 mg/L, Temperature: 25 ^{o}C, TBA=12 mM, p-BQ=12 mM, NaN_3=12 mM.

In the catalytic ozonation processes, reactive radicals such as ·OH, $^1O_2$, $\dot{O}_2^-$ and HO_2· were generated during the decomposition of ozone.[14] Moreover, ozone molecules are also responsible for organic pollutant degradation.[57] In most of the previous studies, it was believed that hydroxyl radicals not only triggered the radical chain reaction, but also played the dominant role in oxidation of aqueous contaminants.[15] However, some studies revealed that other radicals could govern the degradation of organic pollutants.[58, 59] For the reactive species responsible for ozonation using $CaMn_4O_8$ as a catalyst for degradation of 4-nitrophenol, competitive radical tests employing tert-butanol (t-BA), p-benzoquinone (p-BQ) and sodium azide (NaN_3) as quenching agents were carried out. T-BA was a strong radical scavenger for ·OH with a rate constant of 3.8×10^8-7.6×10^8 $M^{-1}s^{-1}$.[24] It reacts rather slowly with ozone at a rate of 3×10^{-5} $M^{-1}s^{-1}$.[60] Fig. 6 presents 4-nitrophenol degradation

profiles in the presence of various quenching agents. At 12 mM t-BA, 4-nitrophenol degradation curve almost overlapped the original one without any quenching agent, revealing a negligible inhibition effect by hydroxyl radicals and suggesting they were not the main reactive species for the catalytic ozonation.

P-BQ has been confirmed to be an effective probe for superoxide radicals ($^{\cdot}O_2^-$).[38, 61] At 12 mM p-BQ, a significant decrease was observed in 4-nitrophenol degradation and only 30% of target pollutant was removed within 1 h, indicating that superoxide radicals played an essential role in the pollutant degradation process.

The singlet $^1O_2$ could be distinguished by addition of sodium azide, possessing a reaction rate of 2×10^9 M^{-1}.[61] At 12 mM NaN_3, 90% of 4-nitrophenol was decomposed in 1 h. Researches showed that sodium azide is also a powerful hydroxyl radical scavenger having a similar reaction rate with singlet $^1O_2$ (2×10^9 M^{-1} vs.1×10^9 $M^{-1}s^{-1}$).[62] However, t-BA test illustrated that ·OH was not the major effective radical for organic pollutant decomposition. Therefore, it is deduced that singlet $^1O_2$ also participated in the catalytic ozonation process.

As discussed above, the addition of p-BQ resulted in a decrease of 4-nitrophenol decomposition by 25%, suggesting superoxide radicals are responsible for about 75% of the degradation of 4-nitrophenol. While the employment of NaN_3 alone led to more than 80% removal of 4-nitrophenol, indicating singlet $^1O_2$ contributed to about 20% of the 4-nitrophenol decomposition. Theoretically, in the presence of both p-BQ and NaN_3 in solution, insignificant amount of 4-nitrophenol would be degraded. However, at 12 mM of p-BQ and 12 mM of sodium azide, 20% of 4-nitrophenol was degraded at the end of the reaction, suggesting that, apart from the reactive radicals, other reactive species also participated in the 4-nitrophenol degradation process. It is well know that O_3 molecule is an effective oxidant with a high redox potential of 2.07 V,[14] which could also contribute to the degradation of the target pollutant.

Competitive radical tests suggested superoxide radical and singlet oxygen are the primary reactive species in Ca-Mn-O/ozone system for 4-nitrophenol degradation. To further

consolidate the deduction, an attempt with electron paramagnetic resonance (EPR) method was performed to investigate whether these two radicals could be directly detected during the catalytic ozonation process or other radicals also involved in the oxidation process. 5,5-Dimethyl-1-pyrroline (DMPO) was employed as the spin trapping agent in EPR experiment for detection of hydroxyl and superoxide radicals by measuring the signals of DMPO-OH adducts and DMPO-OOH adducts, respectively.[16, 63] On the other hand, 2,2,6,6-tetramethyl-4-piperidone (TEMP) was utilized as the spin trapping agent to detect singlet oxygen radical.[64]

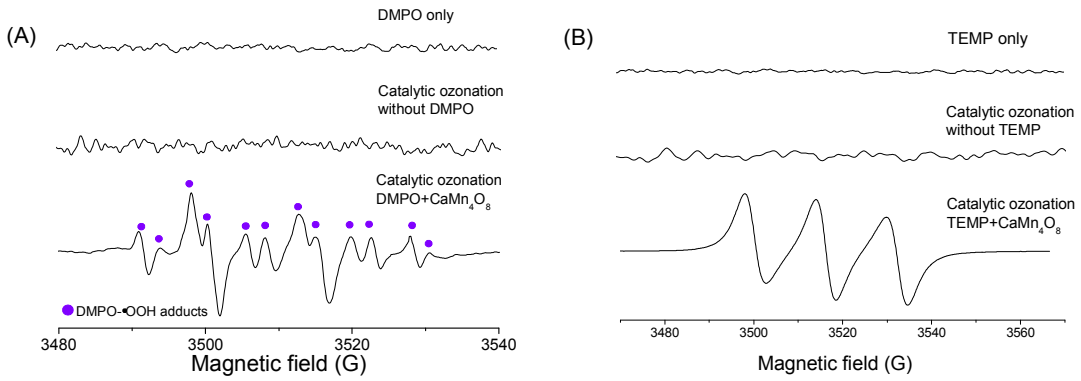

Figure 7. (A) EPR spectra using DMPO as a trapping agent. EPR operating conditions: Centerfield: 3510 G; sweep width: 100 G; microwave frequency: 9.87 GHz; modulation frequency: 100 GHz; and power: 18.11 mW. Catalytic ozonation with DMPO was carried out in absolute ethanol; (B) EPR spectra using TEMP as a trapping agent. EPR operating conditions: Centerfield: 3510 G; sweep width: 100 G; microwave frequency: 9.87 GHz; modulation frequency: 100 GHz; and power: 4.2 mW. Catalytic ozonation with TEMP was carried out in ultrapure water. Reaction conditions: $[4\text{-nitrophenol}]_0$ = 10 mg/L, catalyst loading= 0.2 g/L, Ozone flow rate: 100 mL/min, Ozone loading: 50 mg/L, Temperature: 25 ^{o}C.

Control experiments were firstly carried out to investigate the influence of spin-trapping agents and the self-ozonation on EPR spectra. As seen, no characteristic signals were observed when DMPO and TEMP were tested, suggesting the spin-trapping agents

themselves demonstrated no influence on EPR spectra. Meanwhile, EPR spectra for the catalytic ozonation without the addition of DMPO and TEMP were obtained. Similarly, only plain noise was identified for both the spectra, revealing that without the spin-trapping agent, reactive species cannot be captured to display characteristic signals. To identify the existence of hydroxyl radicals, catalytic ozonation was performed in ultrapure water (ESI, Fig. S15†). With the addition of DMPO, however, no characteristic peaks for DMPO-•OH adducts were identified on the spectrum, indicating no occurrence of hydroxyl radicals during this catalytic ozonation process. Absolute ethanol was employed as the reaction medium instead of ultrapure water to prolong the half-life of superoxide radicals. When 0.1 M of DMPO was added for the catalytic ozonation process, DMPO-•OOH adducts with the hyperfine splitting constants of a_N=14.2 G, a_H^{β}=11.4 G, a_H^{γ}=1.2G were observed,[65] suggesting that superoxide radicals were generated during the catalytic ozonation process employing $CaMn_4O_8$ as a catalyst. However, no characteristic peaks for DMPO-•OH adducts were identified on the spectrum, indicating no generation of hydroxyl radicals during this catalytic ozonation process. To identify singlet oxygen, TEMP (0.05 M) was included in the catalytic ozonation process. As seen (Fig 7(B)), TEMP reacted selectively with singlet oxygen species, producing the stable TEMPO adducts.[66]

With the detection of DMPO-OOH adducts and TEMPO adducts, it was confirmed that superoxide radical and singlet oxygen were generated during the catalytic ozonation process. Hydroxyl radical was excluded in this process due to the non-observation of DMPO-OH adducts. Therefore, superoxide radical and singlet oxygen are the major radicals for 4-nitrophenol degradation.

Therefore, $^{\cdot}O_2^-$, singlet $^1O_2$ and O_3 molecules were responsible for 4-nitrophenol degradation. Moreover, the lower reaction rate in the presence of p-BQ convinced that superoxide radicals was the dominant reactive species for this catalytic ozonation system.

3.4 Effects of electron withdrawing group (EWG) and electron donating group (EDG) on catalytic ozonation process

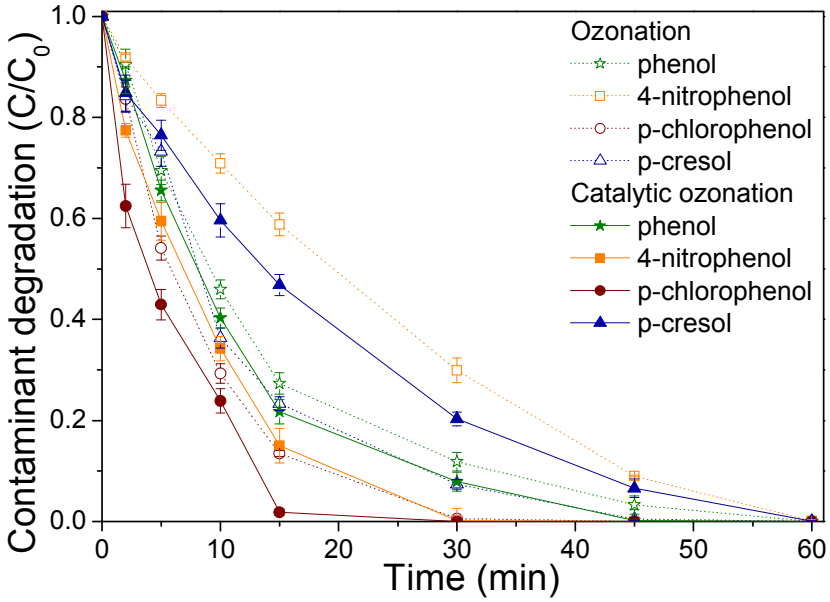

Figure 8. Effects of EWG and EDG on catalytic ozonation process. Reaction conditions: $[4\text{-nitrophenol}]_0$ = 50 ppm, $[phenol]_0$ = 50 ppm, $[p\text{-cresol}]_0$= 50 ppm, $[p\text{-chlorophenol}]_0$= 50 ppm, Catalyst loading = 0.1 g/L, Ozone flow rate: 100 mL/min, Ozone loading: 50 mg/L, Temperature: 25 ^{o}C.

Ozonation/catalytic ozonation process has been proven to be highly effective for decomposition of the phenolic compounds because the strong electrophilic ozone molecules could react directly with nucleophilic position of aromatic rings. [67, 68] It was reported that this reactivity could be influenced by the presence of functional groups on the aromatic rings.[23, 69] Martins et al. found that the substituted electron-donating groups (EDG) such as methyl and hydroxyl groups could enhance the catalytic ozonation efficiency since the electrons from these groups could improve the nucleophilicity of the aromatic rings.[23] While the presence of electron-withdrawing groups (EWG) such as nitro and chloro groups could be beneficial for attracting of nucleophilic reactive species, therefore making the aromatic rings more vulnerable to be attacked.[69]

In order to investigate the effects of EWG/EDG on catalytic ozonation on Ca-Mn-O, nitro group on the para-position of 4-nitrophenol was replaced by methyl (-CH_3, p-cresol) and chloro (-Cl, p-chlorophenol) groups, respectively. In addition, phenol was also tested as the

benchmark (Fig.8). In ozonation tests, 95% decomposition of phenol occurred after 45 min and complete degradation of p-cresol was achieved at the same time. Meanwhile, p-chlorophenol and 4-nitrophenol presented inferior degradation efficiencies, with around 10% and 15% of 4-nitrophenol remained in solution after 45 min, respectively. The ozonation efficiency becomes lower for the target pollutants with a substituted group of higher electronegativity. In the ozonation process, the dominant reactive species for degradation are ozone molecules which favor the electrophilic attack.[70] The presence of EDG on the phenol ring could enhance the electron density of the aromatic ring and make it more vulnerable to be attacked by electrophilic species such as O_3 molecules. Though the nucleophilic species such as superoxide radicals could be formed during the ozonation process, they are too little to influence the whole process. Therefore, the presence of EDG on the target pollutant could improve the efficiency of ozonation.

For catalytic ozonation process, the presence of EDG/EWG produced a different effect from that of ozonation process due to the generation of radicals. The catalytic ozonation of phenol presented complete phenol decomposition in 45 min while p-chlorophenol, 4-nitrophenol and p-cresol were completely degraded within 30 min. p-Chlorophenol showed the highest degradation efficiency. The radical quenching tests suggested that superoxide radicals were the dominant reactive species in catalytic ozonation. Due to the nucleophilicity of the negatively charged superoxide radicals, they are more likely to attack positively charged species.[71] The strong electron withdrawing effect of chloro- and nitro- groups in the aromatic rings of p-chlorophenol and 4-nitrophenol makes them more susceptible to the attack by the superoxide radicals. Fig. 6 also revealed that singlet $^1O_2$ participated in the degradation of target pollutants. Since the produced singlet $^1O_2$ is electrophilic,[72] p-cresol with EDG was more easily to be attacked. Moreover, the electrophilic ozone molecules also accelerated the decomposition of EDG containing p-cresol. Therefore, compared with phenol without substituted groups on para-position, the presence of either EWG or EDG on its para-position could result in the improvement of the catalytic ozonation efficiency due to the nucleophilic attack of superoxide radicals or electrophilic attack of O_3 and singlet $^1O_2$.

4 Conclusions

This study presented a facile fabrication of 3D hierarchically mixed valence $CaMn_3O_6$ and $CaMn_4O_8$ built up from 1D nanorods substructures and their catalytic ozonation performance in 4-nitrophenol degradation and TOC removal. O_3, $\cdot O_2^-$ and $^1O_2$ participated in the catalytic ozonation for 4-nitrophenol degradation, and $\cdot O_2^-$ presented the major contribution. The minor deactivation of the catalysts is mainly derived from the change in surface Mn valence composition. Owing to the nucleophilic attack by superoxide radicals or electrophilic attack by O_3 and singlet $^1O_2$, the presence of either EWG or EDG on the para-position of the aromatic ring could enhance the decomposition of the phenolic compounds in the catalytic ozonation.

Acknowledgements

The authors greatly appreciate the financial supports from the National Natural Science Foundation of China (No. 21207133) and the National Science Fund for Distinguished Young Scholars of China (No. 51425405)

Notes

The authors declare no competing financial interest.

Electronic Supplementary Information

Supplementary Information of EDS, N_2 adsorption, ozone diffusion in solution and kinetic studies in effects of some reaction conditions. The material is available free of charge via the internet at http://xxx.xxx.xx.

Reference

1 P. Yu, X. Zhang, D. Wang, L. Wang and Y. Ma, *Cryst. Growth Des.*, 2009, **9**, 528-533.

2 M.-K. Song, S. Cheng, H. Chen, W. Qin, K.-W. Nam, S. Xu, X.-Q. Yang, A. Bongiorno, J. Lee, J. Bai, T. A. Tyson, J. Cho and M. Liu, *Nano Lett.*, 2012, **12**, 3483-3490.

3 E. Saputra, S. Muhammad, H. Sun, H. M. Ang, M. O. Tadé and S. Wang, *Environ. Sci. Technol.*, 2013, **47**, 5882-5887.

4 W. Xiao, D. Wang and X. W. Lou, *J. Phys. Chem. C*, 2009, **114**, 1694-1700.

5 B. Barrocas, S. Sério and M. E. Melo Jorge, *J. Phys. Chem. C*, 2014, **118**, 24127-24135.

6 X. Han, T. Zhang, J. Du, F. Cheng and J. Chen, *Chem. Sci.*, 2013, **4**, 368-376.

7 M.-J. Lee, S. Lee, P. Oh, Y. Kim and J. Cho, *Nano Lett.*, 2014, **14**, 993-999.

8 Z. I. Bhatti, H. Toda and K. Furukawa, *Water Res.*, 2002, **36**, 1135-1142.

9 S.-P. Sun and A. T. Lemley, *J. Mol. Catal. A: Chem.*, 2011, **349**, 71-79.

10 M. A. Oturan, J. Peiroten, P. Chartrin and A. J. Acher, *Environ. Sci. Technol.*, 2000, **34**, 3474-3479.

11 Y. Wang, H. Sun, X. Duan, H. M. Ang, M. O. Tadé and S. Wang, *Appl. Catal., B*, 2015, **172–173**, 73-81.

12 X. Duan, H. Sun, Y. Wang, J. Kang and S. Wang, *ACS Catal.*, 2015, **5**, 553-559.

13 L. Hu, X. Yang and S. Dang, *Appl. Catal., B*, 2011, **102**, 19-26.

14 B. Kasprzyk-Hordern, M. Ziółek and J. Nawrocki, *Appl. Catal., B*, 2003, **46**, 639-669.

15 J. Nawrocki and B. Kasprzyk-Hordern, *Appl. Catal., B*, 2010, **99**, 27-42.

16 Y. Wang, S. Indrawirawan, X. Duan, H. Sun, H. M. Ang, M. O. Tadé and S. Wang, *Chem. Eng. J.*, 2015, **266**, 12-20.

17 L. Xing, Y. Xie, D. Minakata, H. Cao, J. Xiao, Y. Zhang and J. C. Crittenden, *J. Environ. Sci.*, 2014, **26**, 2095-2105.

18 J. Ma, M. Sui, T. Zhang and C. Guan, *Water Res.*, 2005, **39**, 779-786.

19 R. Gracia, J. L. Aragües and J. L. Ovelleiro, *Ozone Sci. Eng.*, 1996, **18**, 195-208.

20 S. Cortés, J. Sarasa, P. Ormad, R. Gracia and J. L. Ovelleiro, *Ozone Sci. Eng.*, 2000, **22**, 415-426.

21 C.-H. Wu, C.-Y. Kuo and C.-L. Chang, *J. Hazard. Mater.*, 2008, **153**, 1052-1058.

22 H. Cao, L. Xing, G. Wu, Y. Xie, S. Shi, Y. Zhang, D. Minakata and J. C. Crittenden, *Appl. Catal., B*, 2014, **146**, 169-176.

23 R. C. Martins and R. M. Quinta-Ferreira, *Appl. Catal., B*, 2009, **90**, 268-277.

24 H. Zhao, Y. Dong, P. Jiang, G. Wang, J. Zhang, K. Li and C. Feng, *New J. Chem.*, 2014, **38**, 1743-1750.

25 Q. Sun, Y. Wang, L. Li, J. Bing, Y. Wang and H. Yan, *J. Hazard. Mater.*, 2015, **286**, 276-284.

26 E. Saputra, S. Muhammad, H. Sun, H.-M. Ang, M. O. Tadé and S. Wang, *Appl. Catal., B*, 2014, **154–155**, 246-251.

27 Y. Wang, Y. Xie, H. Sun, J. Xiao, H. Cao and S. Wang, *J. Hazard. Mater.*, 2016, **301**, 56-64.

28 Y. Nie, C. Hu, L. Yang and J. Hu, *Sep. Purif. Technol.*, 2013, **117**, 41-45.

29 Q. Sun, Y. Wang, L. Li, J. Bing, Y. Wang and H. Yan, *J. Hazard. Mater.*, 2015, **286**, 276-284.

30 L. Yang, C. Hu, Y. Nie and J. Qu, *Environ. Sci. Technol.*, 2009, **43**, 2525-2529.

31 Y.-C. Hsu, J.-H. Chen and H.-C. Yang, *Water Res.*, 2007, **41**, 71-78.

32 T. C. Wang, G. Qu, J. Li, D. Liang and S. Hu, *Chem. Eng. J.*, 2014, **239**, 178-184.

33 Z. Ryu, J. Zheng, M. Wang and B. Zhang, *Carbon*, 1999, **37**, 1257-1264.

34 J. Hadermann, A. M. Abakumov, L. J. Gillie, C. Martin and M. Hervieu, *Chem. Mater.*, 2006, **18**, 5530-5536.

35 N. Barrier, C. Michel, A. Maignan, M. Hervieu and B. Raveau, *J. Mater. Chem.*, 2005, **15**, 386-393.

36 C. F. Yocum, *Coord. Chem. Rev.*, 2008, **252**, 296-305.

37 J. Limburg, V. A. Szalai and G. W. Brudvig, *J. Chem. Soc., Dalton Trans.*, 1999, DOI: 10.1039/A807583B, 1353-1362.

38 M.-Q. Yang, Y. Zhang, N. Zhang, Z.-R. Tang and Y.-J. Xu, *Sci. Rep.*, 2013, **3**.

39 P. Zhang, Y. Zhan, B. Cai, C. Hao, J. Wang, C. Liu, Z. Meng, Z. Yin and Q. Chen, *Nano Res.*, 2010, **3**, 235-243.

40 E. Saputra, S. Muhammad, H. Sun, H.-M. Ang, M. O. Tadé and S. Wang, *Appl. Catal., B*, 2013, **142–143**, 729-735.

41 M. Abbate, F. M. F. de Groot, J. C. Fuggle, A. Fujimori, O. Strebel, F. Lopez, M. Domke, G. Kaindl, G. A. Sawatzky, M. Takano, Y. Takeda, H. Eisaki and S. Uchida, *Phys. Rev. B: Condens. Matter*, 1992, **46**, 4511-4519.

42 A. Machocki, T. Ioannides, B. Stasinska, W. Gac, G. Avgouropoulos, D. Delimaris, W. Grzegorczyk and S. Pasieczna, *J. Catal.*, 2004, **227**, 282-296.

43 Y. Zhang-Steenwinkel, J. Beckers and A. Bliek, *Appl. Catal., A*, 2002, **235**, 79-92.

44 E. Rezaei and J. Soltan, *Appl. Catal., B*, 2014, **148–149**, 70-79.

45 F. J. Beltrán, V. Gómez-Serrano and A. Durán, *Water Res.*, 1992, **26**, 9-17.

46 J. Hoigné and H. Bader, *Water Res.*, 1983, **17**, 185-194.

47 J. Hoigné and H. Bader, *Water Res.*, 1983, **17**, 173-183.

48 H. Bader and J. Hoigné, *Water Res.*, 1981, **15**, 449-456.

49 M. M. Najafpour, *Dalton Trans.*, 2011, **40**, 3793-3795.

50 J. Yu, K. Huang, H. Wu and P. Li, *Dalton Trans.*, 2012, **41**, 10286-10291.

51 B. Barrocas, S. Sério, A. Rovisco and M. E. Melo Jorge, *J. Phys. Chem. C*, 2014, **118**, 590-597.

52 H. Sun, Y. Wang, S. Liu, L. Ge, L. Wang, Z. Zhu and S. Wang, *Chem. Commun.*, 2013, **49**, 9914-9916.

53 R. Radhakrishnan, S. T. Oyama, J. G. Chen and K. Asakura, *J. Phys. Chem. B*, 2001, **105**, 4245-4253.

54 A. Lv, C. Hu, Y. Nie and J. Qu, *Appl. Catal., B*, 2010, **100**, 62-67.

55 W. Li, G. V. Gibbs and S. T. Oyama, *J. Am. Chem. Soc.*, 1998, **120**, 9041-9046.

56 W. Li and S. T. Oyama, *J. Am. Chem. Soc.*, 1998, **120**, 9047-9052.

57 B. Legube and N. Karpel Vel Leitner, *Catal. Today*, 1999, **53**, 61-72.

58 C. Reed, Y. Xi and S. T. Oyama, *J. Catal.*, 2005, **235**, 378-392.

59 J. Staehelin and J. Hoigne, *Environ. Sci. Technol.*, 1982, **16**, 676-681.

60 G. V. Buxton, C. L. Greenstock, W. P. Helman and A. B. Ross, *J. Phys. Chem. Ref. Data*, 1988, **17**, 513-886.

61 A. Jawad, X. Lu, Z. Chen and G. Yin, *J. Phys. Chem. A*, 2014, **118**, 10028-10035.

62 J. Catalán, C. Díaz and L. Barrio, *Chem. Phys.*, 2004, **300**, 33-39.

63 S. Inoue and S. Kawanishi, *Biochem. Biophys. Res. Commun.*, 1989, **159**, 445-451.

64 É. Hideg, Z. Deák, M. Hakala-Yatkin, M. Karonen, A. W. Rutherford, E. Tyystjärvi, I. Vass and A. Krieger-Liszkay, *Biochim. Biophys. Acta, Bioenerg.*, 2011, **1807**, 1658-1661.

65 K. Reszka, P. Bilski and C. F. Chignell, *Free Radical Res.Commun.*, 1992, **17**, 377-385.

66 V. Gomez-Vidales, G. Granados-Oliveros, A. Nieto-Camacho, M. Reyes-Solis and M. Jimenez-Estrada, *RSC Adv.*, 2014, **4**, 1371-1377.

67 J. Beltran-Heredia, J. Torregrosa, J. R. Dominguez and J. A. Peres, *Water Res.*, 2001, **35**, 1077-1085.

68 F. J. Beltrán, J. F. García-Araya and I. Giráldez, *Appl. Catal., B*, 2006, **63**, 249-259.

69 G. Palmisano, M. Addamo, V. Augugliaro, T. Caronna, E. Garcia-Lopez, V. Loddo and L. Palmisano, *Chem. Commun.*, 2006, DOI: 10.1039/B515853B, 1012-1014.

70 C. Decoret, J. Royer, B. Legube and M. Dore, *Environ. Technol.*, 1984, **5**, 207-218.

71 V. S. Bryantsev, V. Giordani, W. Walker, M. Blanco, S. Zecevic, K. Sasaki, J. Uddin, D. Addison and G. V. Chase, *J. Phys. Chem. A*, 2011, **115**, 12399-12409.

72 N. Kuramoto and T. Kitao, *J. Soc. Dyers Colour.*, 1982, **98**, 334-340.

TOC